AUT Journal of Mechanical Engineering

AUT J. Mech. Eng., 6(1) (2022) 95-112
DOI: 10.22060/ajme.2021.20217.5994

# Fluid-Structure Interaction During Viscoelastic Fluid Hammer Phenomenon in the Pipes

B. Norouzi[1*], A. Ahmadi[2], M. Norouzi[3], M. Lashkarbolouk[4]

[1] Department of Civil Engineering, Lamei Gorgani Institute of Higher Education, Gorgan, Iran
2 Department of Civil Engineering, Shahrood University of Technology, Shahrood, Iran
3 Department of Mechanical Engineering, Shahrood University of Technology, Shahrood, Iran
4 Department of Civil Engineering, Golestan University, Golestan, Iran

**ABSTRACT:** Viscoelastic fluid hammer is a type of fluid hammer in which a viscoelastic non-Newtonian fluid flows in a pipeline. In this study, the fluid-structure interaction in this phenomenon is investigated. The governing equations are viscoelastic fluid and structure equations which are coupled together. Viscoelastic fluid equations consist of continuity and momentum which govern the transitional flow in the pipes. Oldroyd-B model is used as the constitutive equation. This model is suitable for dilute viscoelastic solutions and Boger liquids. Structural equations include pipe axial velocity and stress equations. A two-step variant of the Lax-Friedrichs method is used to simulate fluid-structure interaction in a reservoir-pipe-valve system. A viscoelastic fluid polymer is selected and the behavior of the polymer pressure head and shear stresses during fluid hammer is investigated. Three types of couplings were examined. Junction, Poisson, and the combination of two aforementioned couplings called junction and Poisson coupling. The effects of these couplings for the fluid are modeled in three states. ideally, Newtonian and viscoelastic. The fluid viscosity in Newtonian and viscoelastic states is considered the same. The results of the study show that the imposed shear stresses with viscoelastic fluid are significantly lower than those in the Newtonian state. Comparing coupling effects during fluid hammer is found that the lowest shear stresses are assigned to Poisson coupling.

**Review History:**

Received: Jun. 30, 2021
Revised: Oct. 19, 2021
Accepted:Oct. 20, 2021
Available Online: Oct. 29, 2021

**Keywords:**

Viscoelastic fluid hammer
Oldroyd-B model
Fluid-structure interaction
Junction coupling
Poisson coupling.

## 1- Introduction

Fluid-Structure Interaction (FSI) is an interdisciplinary subject related to fluid dynamics and structural dynamics. In the process of FSI, the solid deforms or moves, forced by the weight of the surrounding fluid. The flow domain then varies according to the deformed or moved solid, which in turn changes the flow field. The first studies in the field of fluid-structure interaction in transient pipe flow were conducted in the 19th century when authors like Korteweg [1] or Helmholtz [2] recognized the need to consider both of the interacting mechanisms of fluid compressibility and pipe-wall distensibility. The classical water-hammer theory is also based on this principle. Since then, many scientists have added their contributions in building up and shaping the theory of hydraulic transients in pipe flow. Skalak [3] inspected the FSI research in the two-way coupling between fluid dynamics and structural mechanics. Wilkinson [4] studied the dynamic response of pipework systems during the water hammer phenomenon and investigated pressure wave behavior in transitional flow. Walker & Phillips [5] a new theory for the propagation of pressure pulses in an inviscid compressible fluid contained in a thin-walled elastic tube was presented. Their new theory was applied to a water-filled copper tube. Valentin et al. [6], analyzed the reflection and transmission of fluid transients at an elbow in the pipe. He coupled fluid and structure equations during the water hammer. Wiggert et al. [7,8] studied fluid-structure Interaction seriously. He analyzed liquid and structural transients in piping using the method of characteristics. In the next study, he introduced coupling equations and coupled transient flow and structural motion in liquid-filled piping systems. Joung & Shin [9], developed a new model on transient wave propagation in fluid-filled tubes. Their new model was taken into account the shear and flexural waves of the elastic tube and Walker-Phillips' theory could be recovered as a special, limiting case. Burmann & Thielen [10], Measured and computed the dynamic reactive forces on pipes containing flow during transitional flow in the pipes. Wiggert & Tijsseling [11] simulated fluid transients and fluid-structure interaction in flexible liquid-filled piping. Their model resulting in improved techniques is readily available to predict FSI and present relevant data that describe the phenomenon. Tijsseling [12] introduced FSI four-equation model. He defined two equations for the liquid which are coupled to two equations for the pipe, through terms proportional to the Poisson contraction ratio, and through mutual boundary conditions. In his model, the exact solutions were used to investigate the error due to numerical interpolations and wave speed adjustments, with emphasis on the latter. Considering the achievements and results from these studies, sub-theories improving the basic assumptions are added, such as unsteady friction [13], pipe-wall viscoelasticity [14], cavitation [15], and the

*Corresponding author's email: norouzi@lameigorgani.ac.ir

effect of different couplings [16]. In this work, the fluid-structure interaction is considered in the case in which, instead of water, a non-Newtonian viscoelastic fluid flows in the pipe, and therefore, this group of equations can be called Viscoelastic Fluid-Structure Interaction (VFSI) which is investigated during Viscoelastic Fluid Hammer. The term Viscoelastic fluid hammer speaks of transients of viscoelastic fluids which are caused by a sudden alteration in the conditions of flow.

Viscoelastic behavior of fluid is dominant in an extensive range of applications including food processing, pharmaceuticals, the casting industry, and the chemical industry. One of the important applications of viscoelastic fluids is in microfluidic devices, for example, microfluidic rectifiers [17] which use viscoelastic materials as working fluid. A great portion of biological fluids in nature display viscoelastic behavior. Thus it is important to understand the dynamics of viscoelastic fluids. In chemical and process industries, it is often required to pump fluids through the pipe from storage to various processing units and/or from one plant site to another and considering issues associated with stopping the flow in the pipe suddenly is necessary. Numerical simulation has become a powerful method in studying the original physics of viscoelastic behavior of fluids and also an important tool in designing and in industrial processes of viscoelastic applications. In numerical simulations, the viscoelastic flow is solved using Navier-Stokes equations integrated with additional constitutive equations which describe the relation of stress with the strain rate tensor [18]. A variation of numerical methods, including finite difference, finite element, finite volume, and hybrid methods, have been developed to simulate viscoelastic flows [19]. In spite of considerable progress in the field of viscoelastic fluid flow, the key questions in the field of non-Newtonian Viscoelastic Fluid-Structure Interaction (VFSI) during the fluid hammer phenomenon have not yet been answered.

According to the literature, the previous studies have been limited to FSI during Newtonian fluid hammer and in the field of VFSI, studies have been focused on situations other than a viscoelastic fluid hammer, and none of them considered the effects of viscoelastic fluid properties on the interaction of fluid and structure. So it appears the realm of VFSI needs to be scrutinized, regarding abrupt valve closure as well as the subsequent phenomena of rising and falling of the transient. The objective of the present study is to investigate the effects of viscoelastic fluid properties on fluid-structure interaction during the viscoelastic fluid hammer phenomenon. To this end, at first, two equations representing the conservation of mass and momentum which govern the transitional flow for non-Newtonian fluids are derived and the Oldroyd-B constitutive equation is used to model the behavior of the viscoelastic fluid. Then, structural equations are written and coupling conditions in junction coupling and Poisson coupling are investigated.

The numerical method used for the discretization of the equations is a two-step variant of the Lax-Friedrichs (LxF) method. It is one of the finite difference methods. The main point in this numerical method, which distinguishes it from other numerical methods, is using multi-step methods. Multi-step methods, which use finite difference relations at split time levels, work well, especially when they are applied to non-linear hyperbolic equations [25]. In this method, firstly, a half time step is taken based on the LxF scheme on a staggered mesh. Then, the second half step is implemented based on LxF to arrive at the solution on the original mesh. High accuracy and convergence, the low computational cost compared to other numerical methods and simple algebraic operation can be expressed as important features of this numerical method.

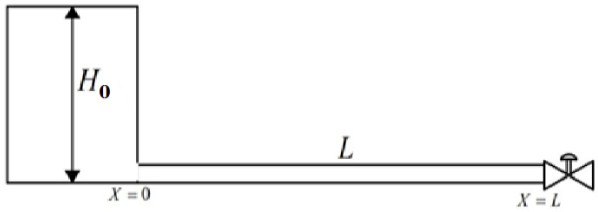


**Fig. 1. Schematic of the reservoir-pipe-valve system [29]**

Computational results are provided in terms of the time history of the pressure head and the ratio of flow shear stresses at critical points of a pipe such as at the valve and mid-length of the pipe. In this study fluid-structure interaction during fluid hammer with viscoelastic fluid in a simple reservoir-pipe-valve system is simulated. Considering the boundary conditions in each coupling, the pressure wave behavior for the fluid is modeled in three different states (ideally, Newtonian and viscoelastic) separately. Investigation and comparison of shear stresses due to the flood hammer phenomenon can be expressed as another highlight of this study. Here, shear stresses at the midpoint of the pipe in FSI and No FSI conditions are calculated in the mention couplings. Also, shear stresses due to viscoelastic fluid are shown and interpreted separately during different couplings.

The schematic shape of the problem is shown in Fig. 1.

Fig. 1 shows that the pipe system consists of a reservoir at the upstream end of the pipeline and a valve at the downstream end discharging to the atmosphere.

## 2- Formulation

In this section, the governing equations for each sub-problem domain and the coupling conditions on the interface are presented.

### 2- 1- Fluid equations

The equations for fluid transients in elastic pipes are continuity and axial momentum. It should be noted that for modeling the problem in one-dimensional form, neglecting the nonlinear convective terms [20], the mentioned equations integrate across the pipe cross-section. Besides, because of

investigating fluid-structure interaction during fluid hammer, it is necessary to replace the proportional term of pipe axial velocity with the radial velocity of the flow in the continuity equation [21].

$$\frac{\partial H}{\partial t}+\frac{c_f{}^2}{g}\frac{\partial \overline{V}}{\partial z}-2\upsilon\frac{\partial \dot{u}_z}{\partial z}\frac{c_f{}^2}{g}=0 \tag{1}$$

$$\frac{\partial H}{\partial t}+\frac{c_f{}^2}{g}\frac{\partial \overline{V}}{\partial z}-2\upsilon\frac{\partial \dot{u}_z}{\partial z}\frac{c_f{}^2}{g}=0 \tag{2}$$

Where $H$ is the pressure head and $t$ is time, $\dot{u}_z$ is axial pipe velocity, $\overline{V}$ is the average cross-sectional velocity, $c_f$ is the wave speed [22]:

$$c_f^2=\frac{\frac{E_f}{\rho_f}}{1+k\frac{E_f D}{eE_p}} \tag{3}$$

$$\overline{V}=\frac{1}{A}\int v_z dA \tag{4}$$

Here, $\rho_f$ is the fluid density, $E_f$ is the bulk modulus of compressibility for the fluid, $E_p$ is Young's modulus of elasticity for the pipe material, $e$ is the pipe thickness and $D$ is the pipe diameter, $v_z$ is axial velocity, $\tau_{rz}$ is the shear stress in the liquid and R is the pipe radius. The coefficient of restriction for axial pipe movement, $k$ is a function of Poisson's ratio for the pipe material, $\upsilon_p$ as follows [22]:

$$k=\begin{cases}1-\dfrac{\upsilon_p}{2} & \text{Pipe restrained at upstream end only}\\ 1-\upsilon_p^2 & \text{Pipe restrained from axial movement}\\ 1 & \text{Pipe with expansion joints}\end{cases} \tag{5}$$

### 2- 1- 1- Constitutive equations

Constitutive equations are a relation between two physical quantities that is specific to a material or substance and approximates the response of that fluids. The Oldroyd-B model is a constitutive model used to describe the flow of viscoelastic fluids. This model can be regarded as an extension of the Upper Convected Maxwell model [23]. In this model, the intended solution is considered as a compound of the Upper Convected Maxwell Model (UCM) polymer and Newtonian solvent. This model can be written as [24]:

$$\boldsymbol{\tau}+\lambda\overset{\nabla}{\boldsymbol{\tau}}=\eta\left(\dot{\boldsymbol{\gamma}}+\theta\overset{\nabla}{\dot{\boldsymbol{\gamma}}}\right) \tag{6}$$

where $\tau$ is the stress tensor, $\eta$ is viscosity, $\lambda$ is relaxation time, $\theta$ is retardation time, and $\nabla$ is the upper convected derivative which is defined as:

$$\overset{\nabla}{\mathbf{A}}=\frac{\mathbf{DA}}{\mathbf{D}t}-\left((\nabla\mathbf{v})^T.\mathbf{A}+\mathbf{A}.(\nabla\mathbf{v})\right). \tag{7}$$

where A is an arbitrary tensor. In Eq. (6), the term $\dot{\gamma}$ is the shear rate and $\overset{\nabla}{\dot{\gamma}}$ is an upper convected derivative of the shear rate defined as:

$$\dot{\boldsymbol{\gamma}}=\left(\nabla\mathbf{v}\right)+(\nabla\mathbf{v})^T \tag{8a}$$

$$\overset{\nabla}{\dot{\boldsymbol{\gamma}}}=\frac{D\dot{\boldsymbol{\gamma}}}{Dt}-\left((\nabla\mathbf{v})^T.\dot{\boldsymbol{\gamma}}+\dot{\boldsymbol{\gamma}}.(\nabla\mathbf{v})\right). \tag{8b}$$

where $\frac{D\dot{\gamma}}{Dt}$ is a complete derivative of polymer shear stress tensor, $\nabla\mathbf{v}$ is velocity gradient, and $T$ is transpose operator. The Oldroyd-B model is usually considered for a polymeric solution in which the polymeric additives with the upper-convected Maxwell model (UCM) are solved in a Newtonian solvent. Therefore, the stress of the Oldroyd-B model can be expressed as

$$\boldsymbol{\tau}=\boldsymbol{\tau}_p+\boldsymbol{\tau}_s \tag{9a}$$

$$\boldsymbol{\tau}_p+\lambda\overset{\nabla}{\boldsymbol{\tau}}_p=\eta_p\dot{\boldsymbol{\gamma}} \tag{9b}$$

$$\boldsymbol{\tau}_s=\eta_s\dot{\boldsymbol{\gamma}} \tag{9c}$$

where subscripts s and p denote the Newtonian solvent and polymeric additives, respectively.

It can easily be shown that the above statement of the Oldroyd-B model (Eq. (6)) is identical with Eq. (9) by considering the following relations:

$$\eta=\eta_s+\eta_p \tag{10a}$$

$$\theta=\frac{\eta_s}{\eta_s+\eta_p}\lambda=(1-\beta)\lambda \tag{10b}$$

where $\beta$ is viscosity ratio and defined as:

$$\beta = \eta_P / \eta \tag{11}$$

Regarding Eq. (10), we have:

$$\tau_{rz}\big|_{r=R} = \tau_{srz}\big|_{r=R} + \tau_{prz}\big|_{r=R} \tag{12}$$

$$\tau_{srz}\big|_{r=R} = \eta_s(\nabla \mathbf{v} + (\nabla \mathbf{v})^T)_{rz} = \eta_s\left(\frac{\partial v_z}{\partial r} + \frac{\partial v_r}{\partial z}\right)\Big|_{r=R} \tag{13}$$

$$\tau_{prz}\big|_{r=R} + \lambda \overset{\nabla}{\tau}_{prz}\Big|_{r=R} = \eta_p\left(\frac{\partial v_z}{\partial r} + \frac{\partial v_r}{\partial z}\right)\Big|_{r=R} \tag{14}$$

To replace shear stress in the momentum equation, at first, the velocity distribution profile equation for laminar flow in a pipe must be considered:

$$v_z = v_{z\max}(1 - \frac{r^2}{R^2}) \tag{15}$$

Where $r$ is the radial distance from the pipe center. In fact, considering the Poiseuille velocity distribution profile equation for laminar flow in a long pipe and replacing the appropriate values in Eqs. (13) and (14), the shear stress $\tau_{rz}\big|_{r=R}$ is obtained. So, the governing equations for visco-elastic fluid hammer are given by:

$$\frac{\partial \bar{V}}{\partial t} + g\frac{\partial H}{\partial z} - \frac{2}{\rho R}(\tau_{srz}\big|_{r=R} + \tau_{prz}\big|_{r=R}) = 0 \tag{16}$$

$$\tau_{srz}\big|_{r=R} = -\eta_s.\frac{4\bar{V}}{R} \tag{17}$$

$$\tau_{prz}\big|_{r=R} + \lambda\frac{\partial \tau_{prz}}{\partial t} = -\eta_p\frac{4\bar{V}}{R} \tag{18}$$

Replacing zero for polymer terms in the momentum equation, classical water-hammer equations are achieved.

## 2- 2- Structural equations

The governing equation for the axial motion of the pipe is a two-order equation. This equation can be transformed into two first-order equations [16]:

$$\frac{\partial \dot{u}_z}{\partial t} - \frac{1}{\rho_t}\frac{\partial \sigma_z}{\partial z} = 0 \tag{19}$$

$$\frac{\partial \dot{u}_z}{\partial z} - \frac{1}{\rho_t c_t^2}\frac{\partial \sigma_z}{\partial t} + g\frac{D}{2}\frac{\upsilon_p \rho_f}{e\rho_t c_t^2}\frac{\partial H}{\partial t} = 0 \tag{20}$$

$$\rho_t c_t^2 = E_p \tag{21}$$

In which:

where $u_z$ is pipe axial velocity, $\sigma_z$ is the pipe axial stress, $\rho_t$ is the density of pipe wall material, and $c_t$ is axial stress wave speed.

### 2.3. Non-dimensionalization of the equations

Considering the above dimensionless groups, the non-dimensional fluid and structure equations can be expressed as follows:

$$\frac{\partial H^*}{\partial t^*} + \frac{\partial \bar{V}^*}{\partial z^*} - 2\upsilon\frac{\partial \dot{u}_z^*}{\partial z^*} = 0 \tag{22}$$

$$\frac{\partial \bar{V}^*}{\partial t^*} + \frac{\partial H^*}{\partial z^*} - 4(\bar{\tau}^*_{srz} + \bar{\tau}^*_{prz}) = 0 \tag{23}$$

$$\bar{\tau}^*_{srz} = \frac{-8}{\mathrm{Re}}.M.\bar{V}^*.(1-\beta) \tag{24}$$

$$\bar{\tau}^*_{prz} + \frac{De}{M}.\frac{\partial \bar{\tau}^*_{prz}}{\partial t^*} = -8\beta.\frac{\bar{V}^*}{\mathrm{Re}}.M \tag{25}$$

$$\frac{\partial \dot{u}_z^*}{\partial t^*} - \frac{1}{c^*}\frac{\partial \sigma_z^*}{\partial z^*} = 0 \tag{26}$$

$$\frac{\partial \sigma_z^*}{\partial t^*} - \frac{1}{c^*}\frac{\partial \dot{u}_z^*}{\partial z^*} - c^* D^* \rho^* \frac{\upsilon_p}{2}\frac{\partial H^*}{\partial t^*} = 0 \tag{27}$$

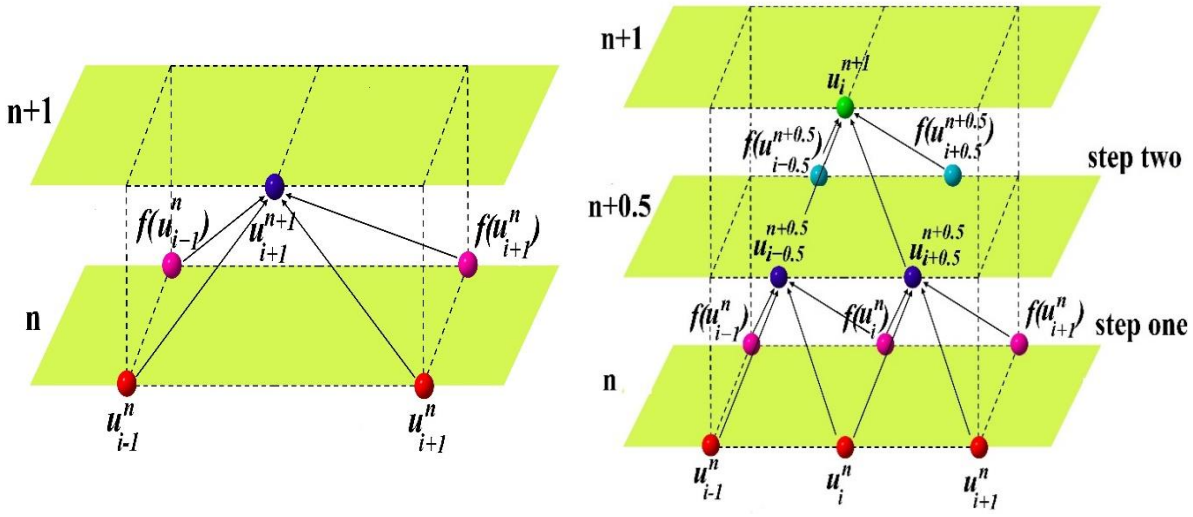


**A.** One-step LxF **B**. Two-step LxF

**Fig. 2. Stencil of LxF method [16]**

where $De$ denotes Deborah number which is attributed to an important feature of viscoelastic fluid called relaxation time constant, $\beta$ is the viscosity ratio to show the magnitude of polymer viscosity with respect to the total viscosity, $M$ is Mach number and Re is Reynolds number. In the case of a Newtonian fluid, the above equations are rewritten by substituting $\beta = 0, De = 0$.

## 3- Numerical Method

The Lax–Friedrichs (LxF) method is a simple method for solving partial differential equations. The basis of this method is the Finite Difference Method (FDM). The finite difference method works by replacing the region over which the independent variables in the Partial Differential Equations (PDEs) are defined by a finite grid of points at which the dependent variable is approximated. LxF method is available for all forms of PDEs [25]. Generally, multi-step methods increase convergence and accuracy in numerical problems. In this study, a two-step variant of the LxF method is used. In this method, firstly, a half time step is taken based on LxF scheme on a staggered mesh. Next, the second half step is implemented based on LxF to reach the solution on the original mesh. In Fig. 2, the stencil of conventional LXF and two-step LxF are plotted.

Fig. 2 shows that in the two-step LxF method, a one-time step is divided into two halves. In part A, to calculate the amount of the variable in the next time step $u_i^{n+1}$, it is enough in the present time step to have the values $u_{i-1}^n, u_{i+1}^n$ to calculate the amount of the variable in the next time step $u_i^{n+1}$ immediately. Now in part B, if the time and space interval on the way to the next time step is divided into two halves, the equations become a little more complicated, however, the results are more convergent and more accurate.

The equations are discretized as follows in the first time step:

$$\frac{u_{i+\frac{1}{2}}^{n+\frac{1}{2}} - \frac{1}{2}(u_{i+1}^n + u_i^n)}{\frac{\Delta t}{2}} = \frac{f(u_{i+1}^n) - f(u_i^n)}{2\frac{\Delta x}{2}}$$
$$u_{i+\frac{1}{2}}^{n+\frac{1}{2}} = \frac{1}{2}(u_{i+1}^n + u_i^n) + \frac{\Delta t}{2}\left(\frac{f(u_{i+1}^n) - f(u_i^n)}{\Delta x}\right) \quad (28)$$

Note that using the above equation, the value of the function $u$ is obtained in spatial nodes $i = 1,2,...,M-1$ at a time $n+\frac{1}{2}$.

Now the equations are discretized in the second time step as follows:

$$\frac{u_i^{n+1} - \frac{1}{2}\left(u_{i+\frac{1}{2}}^{n+\frac{1}{2}} + u_{i-\frac{1}{2}}^{n+\frac{1}{2}}\right)}{\frac{\Delta t}{2}} = \frac{f(u_{i+\frac{1}{2}}^{n+\frac{1}{2}}) - f(u_{i-\frac{1}{2}}^{n+\frac{1}{2}})}{2\frac{\Delta x}{2}}$$
$$u_i^{n+1} = \frac{1}{2}\left(u_{i+\frac{1}{2}}^{n+\frac{1}{2}} + u_{i-\frac{1}{2}}^{n+\frac{1}{2}}\right) + \frac{\Delta t}{2}\left(\frac{f(u_{i+\frac{1}{2}}^{n+\frac{1}{2}}) - f(u_{i-\frac{1}{2}}^{n+\frac{1}{2}})}{\Delta x}\right) \quad (29)$$

In this way, the values of the function $u$ in the nodes of space $i = 1,2,...,M-1$ on the main mesh at a time $n+1$ are obtained. Note that in this state, at the first step, the values of

**Table 1. Properties and pipe configuration data [26]**

| properties | Values |
|---|---|
| Pipe length (m) | 36.09 |
| Mean velocity (m/s) | 0.128 |
| Pressure wave speed (m/s) | 1324 |
| Pipe diameter (m) | 0.0253 |
| Darcy-Weisbach friction factor | 0.78 |
| Specific density of fluid (kg/m$^3$) | 878 |
| Dynamic Viscosity (Pa.s) | 0.03483 |

the function for example $U$ in spatial nodes $i = 1, 2,...,v - 1$ and the time $n + 0.5$ on a grid mesh is obtained where $v$ is the node in the place of the valve, and in the second half step, the values of the mention function in spatial nodes $i = 2, 3,...,v - 1$ and the time $n + 1$ on the original mesh is achieved. We know the stability condition is $\frac{c\Delta t}{\Delta x} \le 1$ and c is pressure wave speed. In this one-dimensional simulation, the stability condition and the Non-dimensional spatial step size for the grid $(\frac{\Delta x}{l})$ are considered 0.99 and 0.001 respectively.

## 4- Validation of the Present Numerical Model

Because of the lack of texts on experimental works about the fluid hammer with viscoelastic fluid in the pipes, it was decided that in the first step, the result of the present study is validated by laboratory data for a Newtonian fluid in the pipe. It is important to mention that verifying the Computational Fluid Dynamics (CFD) simulation of non-Newtonian flows with special Newtonian cases is usual in rheology and non-Newtonian fluid mechanics which is mostly related to the dearth of experimental data. In other words, the CFD code is verified as a special Newtonian case by considering zero relaxation time. Holmboe and Rouleau's experiment [26] is chosen as a valid laboratory sample in the field of fluid hammer phenomenon in the pipe. The properties and pipe configuration data are presented in Table 1. In this experiment, the fluid transient is generated by the sudden closure of the downstream valve.

Among the numerical studies that have modeled fluid hammer phenomenon in the pipe using different numerical methods, in the present paper, Wahba's study in the one-dimensional state [20] for validation of the proposed model is selected. Wahba [20] studied laminar transitional flows in the pipeline in one and two-dimensional states. In his study, Runge–Kutta schemes were used to simulate unsteady flow in elastic pipes due to sudden valve closure, and the spatial derivatives were discretized using a central difference scheme. In this numerical modeling, also, Holmboe and Rouleau's experiment [26] data have been used.

In the present study, the modeling has been done one-dimensional, so it is expected that after ignoring the non-Newtonian terms related to the viscoelastic fluid in the equations, the results of the proposed model for Newtonian fluid using the LxF method are well suited to the results of the mentioned studies. The initial conditions in Holmboe and Rouleau experiment [26] are taken according to the steady-state situation of the system. The boundary conditions describe the situation at the pipe ends, where for instance a reservoir or valve is located. The boundary conditions that describe a constant head reservoir with a pipe rigidly connected to it is $H = H_0$ where subscript $0$ shows the value of variables in the steady state situation of the system, and a zero velocity boundary condition is imposed at the downstream end to simulate the abrupt closure of the valve. Fig. 3 shows a comparison between the results obtained using Wahba (1-D) [20] with the proposed model using the LxF method and experimental results.

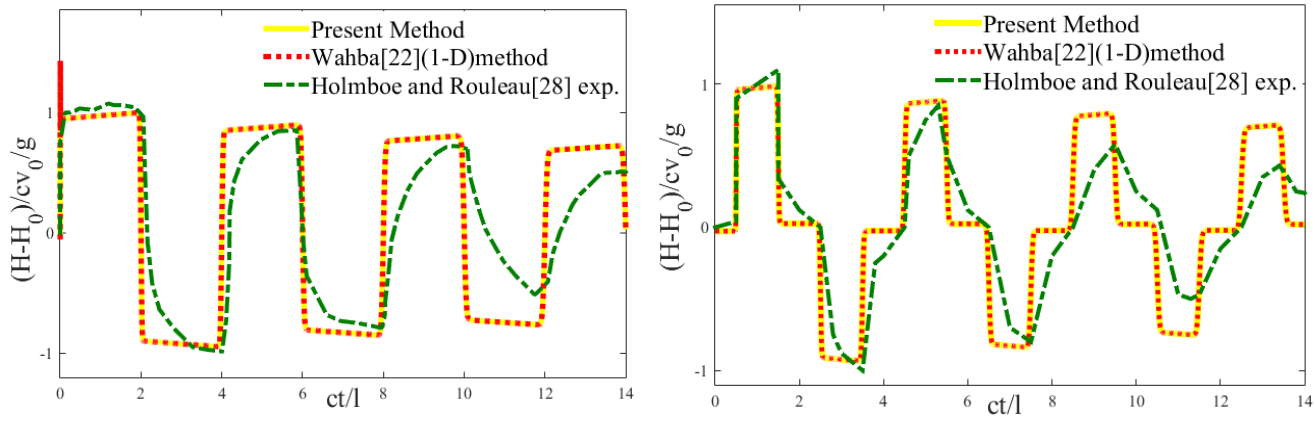


**A. At valve point** **B. At midpoint**

**Fig. 3. Pressure- time history**

**Table 2. The spectrum of relaxation time and viscosity [27]**

| Mode No. | Dynamic Viscosity (Pa.s) | Relaxation time constant (s) |
|---|---|---|
| 0 | 0.0319 | 0 |
| 1 | 0.0625 | 7.088E-4 |
| 2 | 0.0131 | 0.2469 |
| 3 | 0.0025 | 10.2117 |
| 4 | 0.0151 | 9.9311 |

$$\bar{\lambda} = \frac{\sum_1^4 \eta_i \lambda_i}{\sum_1^4 \eta_i} = 1.9\,\mathrm{s}$$

**Table 3. Properties and pipe configuration data**

| Fluid & pipe configuration data | Values |
|---|---|
| Pipe length (m) | 36.09 |
| Mean velocity (m/s) | 0.128 |
| Pressure wave speed (m/s) | 1324 |
| Viscosity (Pa.s) | 0.08918 |
| Pipe's diameter (m) | 0.0253 |
| Solution's density (kg/m$^3$) | 2020 |
| Stress wave speed (m/s) | 5280.5 |
| Pipe's density (kg/m$^3$) | 7900 |
| Young's modulus (GPa) | 210 |
| Poisson's ratio | 0.3 |
| Reynolds number | 80 |
| Viscosity ratio | 0.6 |
| Mach number | 9.66e-5 |
| Deborah number | 10 |

According to Fig. 3, there is a good agreement between the results of the proposed model using the present method and previous numerical works. It is noted that the 1D simulation state of the Wahba [20] method for validation of the present method is considered. The experimental results do not match the numerical results in some points. The reason for that can be attributed to the modeling of the problem one-dimensionally [20]. The 1-D model provides an excellent prediction of the magnitude of the first pressure peak. On the contrary, it underestimates the attenuation of the following pressure peaks resulting in much higher simulated pressure values than those experimentally observed. The reason for this is the inadequate representation of the frictional damping mechanism in the 1-D model [20].

## 5- Numerical Simulation

Pipe systems experience severe dynamic forces during a viscoelastic fluid hammer event. In order to obtain the results near to the physical conditions, we used the properties of a dilute polymeric solution and a real geometry to obtain the typical dimensionless groups. For this purpose, a solution of polyacrylamide (100ppm (0.01 $wt\%$)) in a $80/20$ ($v/v$) glycerin/de-ionized water is considered a typical viscoelastic fluid. The molecular weight of polyacrylamide is $M_w = 5\times10^6\,\mathrm{g/mol}$ and the degree of purity of glycerin is 99%. The viscometric test of this solution indicates that the viscosity has a constant value of $0.08918$ Pa.s in a wide range of shear rate [27] so it could be considered as a Boger liquid and the Oldroyd-B constitutive equation is suitable to describe the mechanical behavior of this solution. The results of curve fitting of four modes generalized Maxwell model on the data of sweep frequency test at constant 10% of strain are presented in Table 2 [27]. Here, mode zero indicates the Newtonian contribution of the model. Based on the data of this table, the fluid has an average relaxation time of 1.9s [27].
In Fig. 4 the comparison between ideal solution (frictionless solution) and Newtonian and viscoelastic solution with similar viscosity is shown. The other properties and pipe

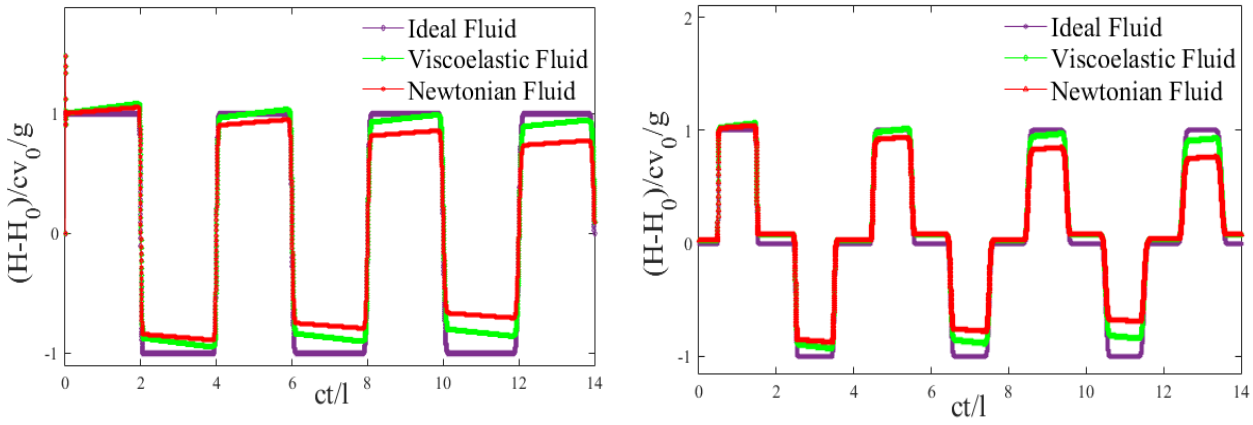


**A. At valve point** **B. At midpoint**

**Fig. 4. The comparison of pressure time history during fluid hammer with different solutions (No FSI)**

**Newtonian Fluid** $\mathrm{Re}=80, \beta=0, M=9.66e-5, De=0$

**Viscoelastic Fluid** $\mathrm{Re}=80, \beta=0.6, M=9.66e-5, De=10$

configuration data are presented in Table 3. The Reynolds number for this laminar flow case is 80, the viscosity ratio is considered 0.6, and Deborah number in the mentioned viscoelastic solution according to the data of Tables 1 and2 is equal to $9.6 \approx 10$ and the fluid transient is generated by the sudden closure of the downstream valve.

The first point in Fig. 4 is related to the pipeline packing or line packing phenomenon [28]. Shortly, in this phenomenon, the value of transient pressure continues to rise above the Joukowsky pressure value due to frictional effects at the valve. The second point is to compare the attenuation time of the pressure wave in these three types of fluid. As it is known, in the ideal fluid, damping does not occur for the transition flow because the viscosity of the fluid is considered zero. Fig. 4 also shows that the height of the transitional flow in the viscoelastic solution compared to the Newtonian solution is higher which leads to a longer attenuation time. This issue must be referred to the viscoelastic properties of the fluid. In a Newtonian fluid, after the imposition of the potential energy caused by the sudden closure of the valve, the viscous characteristic of the liquid damps the pressure wave gradually. In a viscoelastic fluid, solid and liquid properties, show different reactions to this sudden potential energy at the same time. In fact, a viscoelastic solution has viscous and elastic properties simultaneously. The elastic property plays an important role in storing the potential energy imposed on the fluid, while the viscous part is extremely eager to waste the imposed energy. Finally, these different actions in a viscoelastic fluid cause the damping time of the transition flow to become longer compared to Newtonian fluid [29, 30].

## 6- Numerical Results of Fluid-Structure Interaction

The interaction is always caused by dynamic forces which act simultaneously on fluid and pipe.

Two important coupling mechanisms during the fluid hammer phenomenon, which are commonly considered as the most common kind of fluid and structure coupling, are junction coupling and Poisson coupling. Poisson coupling is distributed along the axis of a pipe element and acts along with the entire piping system while the junction coupling forces act locally at geometric irregularities such as elbows, tees, orifices, or valves. As follows, the effects of each of the couplings on pressure time history during fluid hammer in different conditions of fluid such as Frictionless (Ideal), Newtonian and Viscoelastic are investigated and compared with no couplings.

### 6- 1- unction coupling

Junction coupling is created from the reactions set up by unbalanced pressure forces and by changes in liquid momentum only at specific places such as elbows, tees, orifices, or valves. It is considered through the boundary conditions or more accurately through the closure relations derived for arbitrarily shaped piping systems.

### 6- 1- 1- . Boundary condition

The initial conditions are taken according to the steady-state situation of the system. The boundary conditions that describe a constant head reservoir with a pipe rigidly connected to it, are [30]:

$$H_1^{n+1} = H_0 \tag{30}$$

$$\dot{u}_{z1}^{n+1} = 0 \tag{31}$$

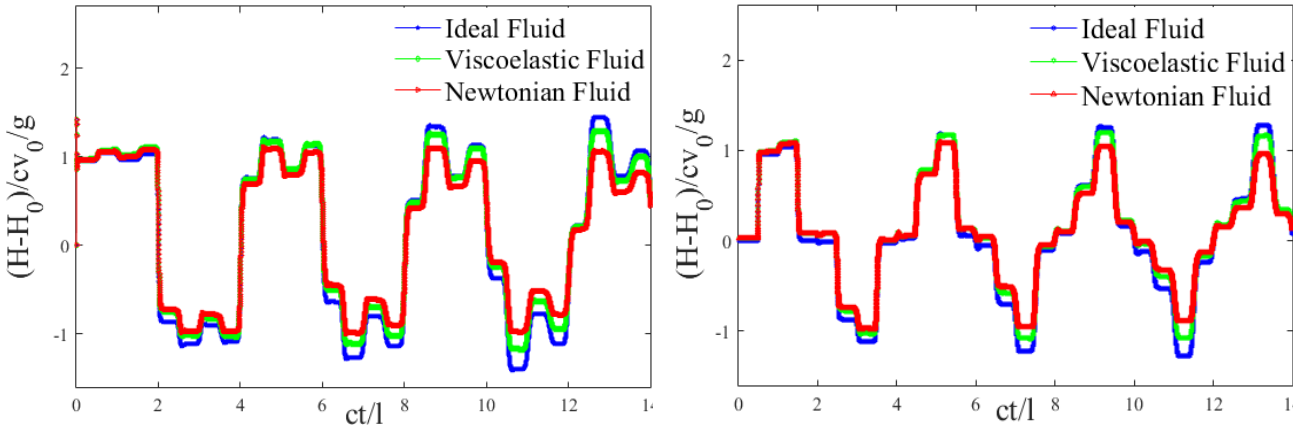


**A. At valve point** **B. At midpoint**

**Fig. 5. The comparison of pressure time history in the condition of FSI junction coupling**

**Newtonian Fluid** $\mathrm{Re}=80, \beta=0, M=9.66e-5, De=0$

**Viscoelastic Fluid** $\mathrm{Re}=80, \beta=0.6, M=9.66e-5, De=10$

Subscript 0 shows the value of variables in the steady-state situation of the system. In Junction coupling, the Poisson's ratio is zero. Boundary conditions at the valve point are as follows:

$$\overline{V}_v^{n+1} = \dot{u}_{zv}^{n+1} \tag{32}$$

$$\sigma_v^{n+1} A_t = \rho_f g A_f (H_v^{n+1} - H_0) \tag{33}$$

Where $A_f$ and $A_t$ are cross-sectional discharge area and cross-sectional pipe wall area respectively. Subscript $v$ refers to the value of variables in the valve. In fact, in junction coupling, the valve is allowed to move and it follows the pipe vibration. In Fig. 5 the comparison between pressure time history in the condition of FSI junction coupling in different states such as ideal, Newtonian, and viscoelastic for fluid during fluid hammer is shown.

In Fig. 5, two mention points in Fig. 4 related to line packing at the valve at t*=0 to t*=2 and attenuation time of the pressure wave in the Newtonian and viscoelastic fluid can be observed. In order to investigate the effects of each coupling on pressure time history in Figs. 6 to 8, the comparisons between FSI and No FSI conditions for each fluid are shown separately.

Figs. 6 to 8 show that the pressure rise created by closing the valve abruptly, pushes the valve in the downstream direction, so extra storage is created for the liquid which results in a lower initial pressure rise. In fact, the movement of the valve causes the fluid to not completely stop and moves at the velocity of the valve. The axial stress wave created by the movement of the valve along the pipe pulls the valve back and this pumping action continues [31].

### 6- 2- Poisson coupling

Poisson coupling is related to the pressures in the fluid to the axial stresses in the pipe via the contraction or expansion of the pipe wall. The pressure waves in the fluid are coupled with axial and radial stress waves in the structure through changes of the pipe cross-section (hoop stress). Poisson coupling is figuratively known as pipe breathing. An interesting and important side effects of the Poisson coupling are precursor waves. The origin of the precursor waves are axial and hoop stress waves in the pipe wall, while changes of pipe cross-section or length, through Poisson coupling, yield to changes in pressure in the fluid. Precursor waves travel faster than pressure waves in the fluid and are thus forerunners of the fluid hammer.

#### 6- 2- 1- Boundary condition

The boundary conditions that describe a constant head reservoir with a pipe rigidly connected to it can be stated as follows:

$$H_1^{n+1} = H_0 \tag{34}$$

$$\dot{u}_{z1}^{n+1} = 0 \tag{35}$$

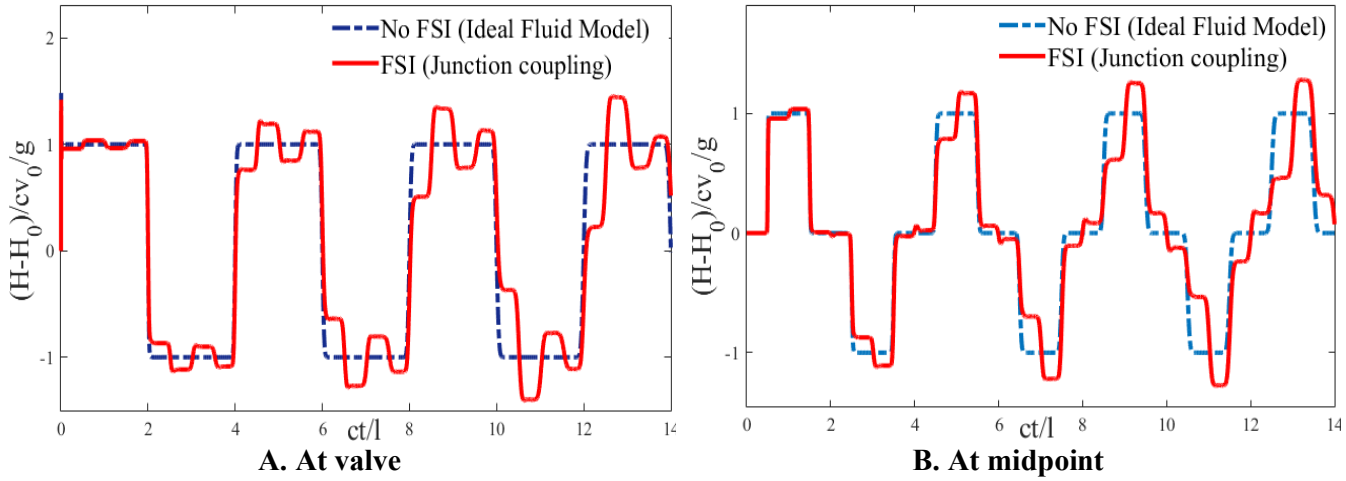


**Fig. 6. Pressure time history during fluid hammer with ideal fluid**

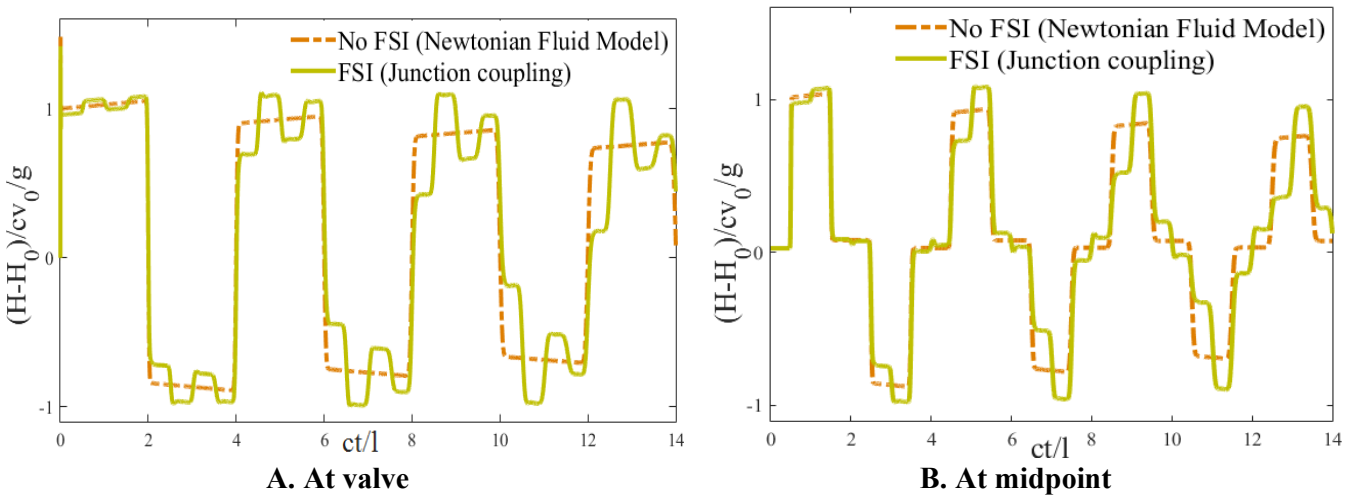


**Fig. 7. Pressure time history during fluid hammer with Newtonian fluid**

$$\mathrm{Re}=80,\beta=0,De=0,M=9.66e-5$$

For the boundary conditions at the valve, a zero velocity boundary condition is imposed at the downstream end to simulate the abrupt closure of the valve.

$$\overline{V}_v^{n+1}=0 \tag{36}$$

$$\overset{\bullet}{u}{}_{zv}^{n+1}=0 \tag{37}$$

According to the boundary conditions, in the Poisson coupling, unlike junction coupling, it is assumed that the valve is fixed. In Fig. 9 the comparison between pressure time history in the condition of FSI Poisson coupling in the mentioned fluids is shown.

In Fig. 9, line packing can be observed at the valve at t*=1 to t*=2. Moreover, in this coupling like junction coupling, the ideal fluid has the largest and the Newtonian fluid has the lowest pressure wave head. In Figs. 10 to 12, the comparisons between FSI and No FSI conditions for each fluid are shown separately.

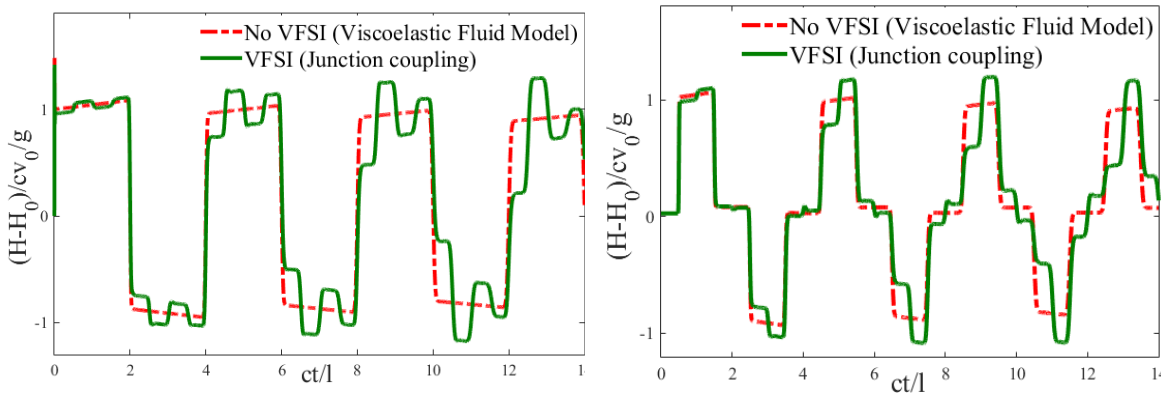


**A. At valve** **B. At midpoint**

**Fig. 8. Pressure time history during fluid hammer with a viscoelastic fluid**

$\mathrm{Re}=80, \beta=0.6, De=9.5, M=9.66e-5$

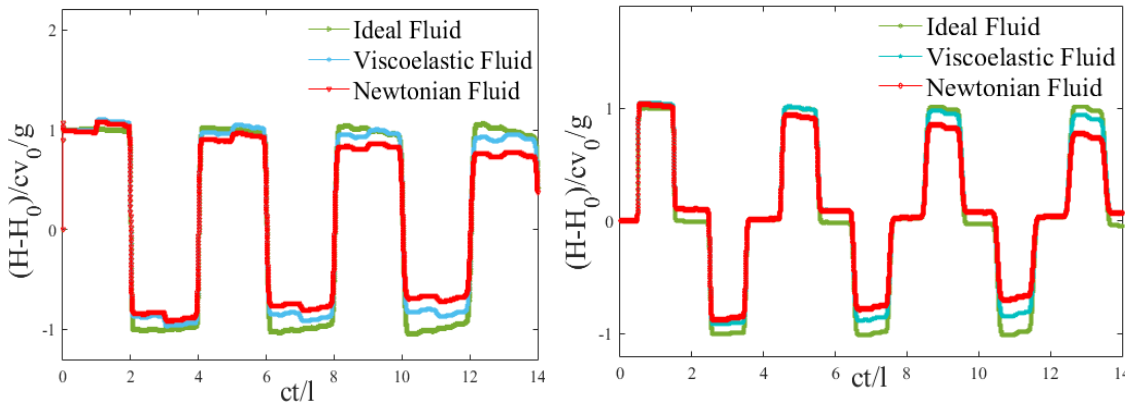


**A. At valve point** **B. At midpoint**

**Fig. 9. The comparison of pressure time history in the condition of FSI Poisson coupling**

**Newtonian Fluid** $\mathrm{Re}=80, \beta=0, M=9.66e-5, De=0$

**Viscoelastic Fluid** $\mathrm{Re}=80, \beta=0.6, M=9.66e-5, De=10$

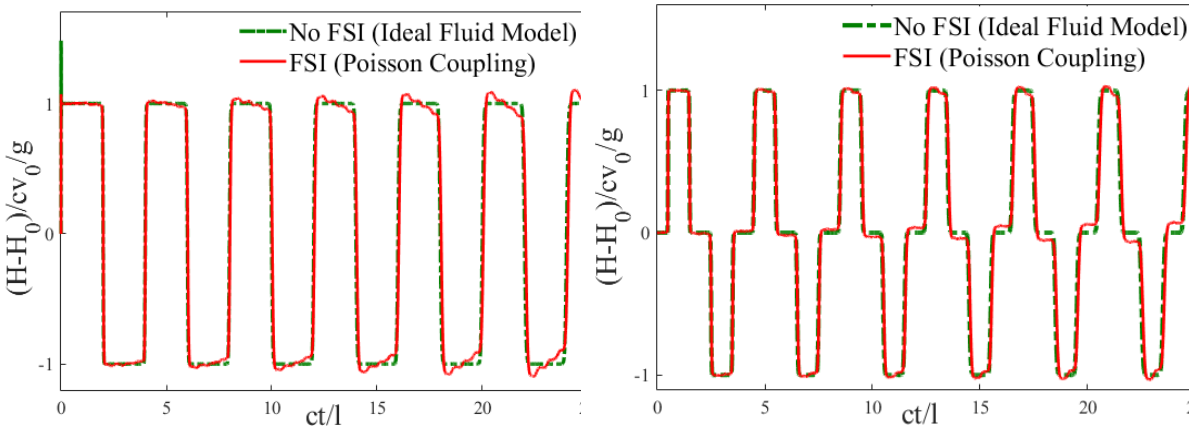


**A. At valve** **B. At midpoint**

**Fig. 10. Pressure time history during fluid hammer with ideal fluid**

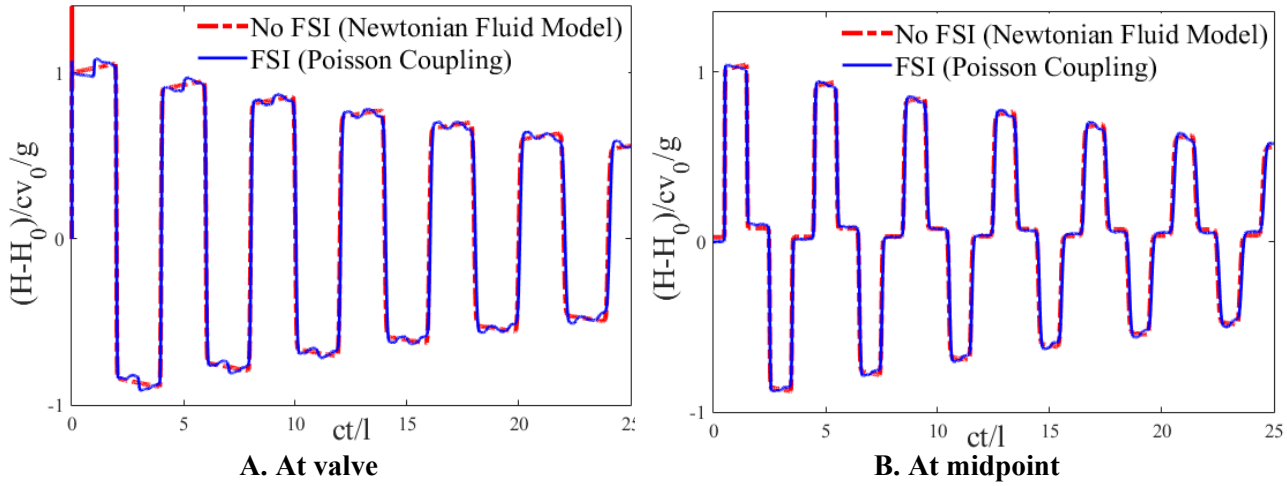


**Fig. 11. Pressure time history during fluid hammer with Newtonian fluid**

$\mathrm{Re}=80, \beta=0, De=0, M=9.66e-5$

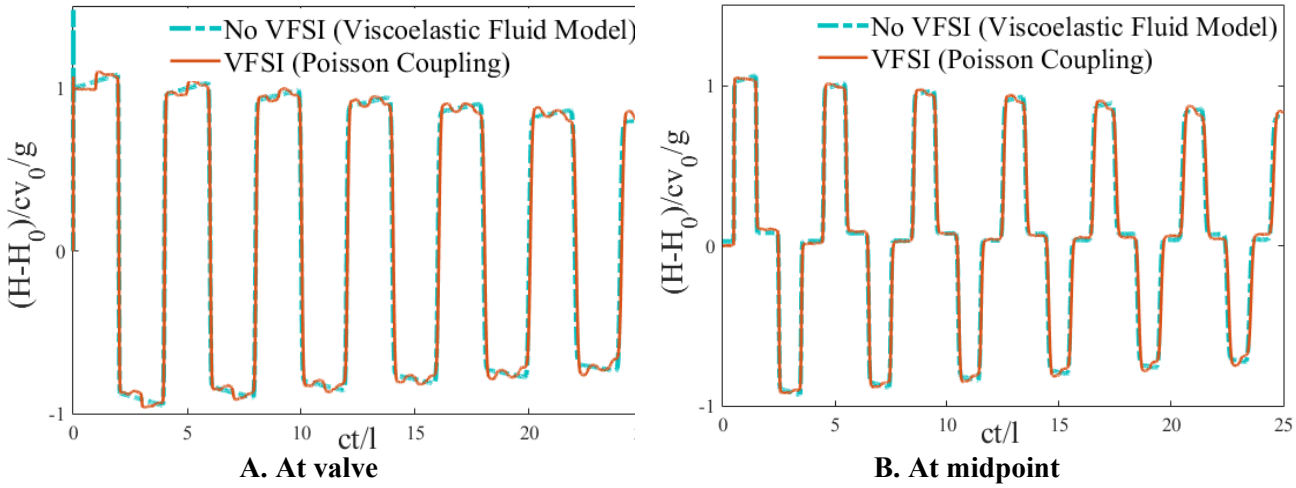


**Fig. 12. Pressure time history during fluid hammer with viscoelastic fluid**

$\mathrm{Re}=80, \beta=0.6, De=10, M=9.66e-5$

Figs. 10 to 12 show that the Poisson coupling has a weak effect on the pressure head at the initial periods of the fluid hammer. The Poisson coupling performance mechanism can be defined as follows: The sudden closure of the valve increases the pressure of the moving fluid causing the radial expansion of the pipe wall. Simultaneously, with radial expansion in the pipe, an axial contraction occurs in the pipe. The axial contraction of the pipe causes a stress wave to be sent which results in a change in pressure in the fluid. As can be seen in Figs. 11 to 13, these effects are very small at first and gradually increase along the pipe.

### 6- 3- Poisson and junction coupling

In this kind of coupling, Poisson equations with junction boundary conditions are imposed on the system and the effect of the sudden closure of the valve on pressure time history during fluid hammer at valve and midpoint is investigated. This result is shown in Fig. 14.

Fig. 13 shows that the fluid's behavior in this coupling is a combination of the previous ones. In Figs. 14 to 16, the comparisons between FSI and No FSI conditions for each fluid are shown separately.

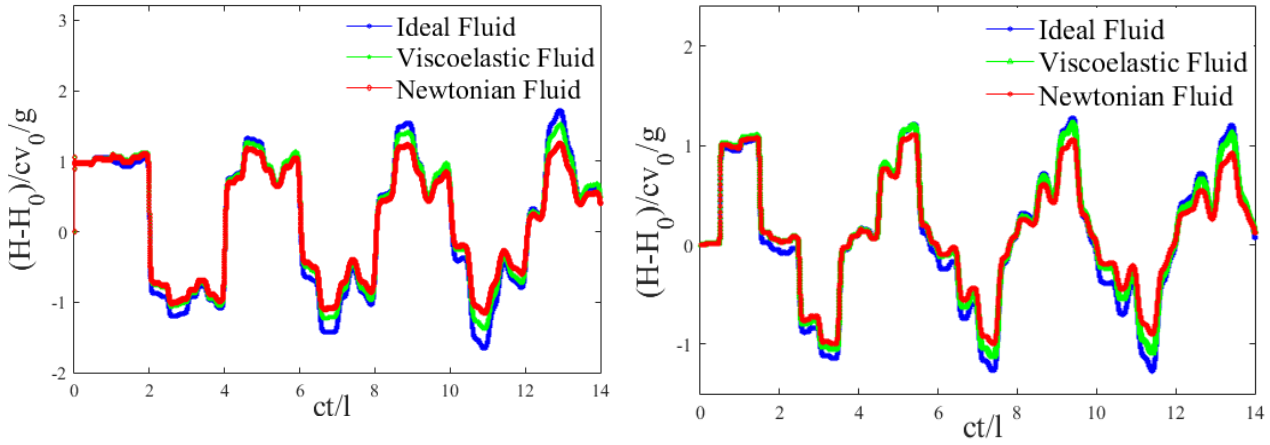


**A. At valve point** **B. At midpoint**

**Fig. 13. The comparison of pressure time history in the condition of FSI junction and Poisson coupling**

**Newtonian Fluid** $Re = 80, \beta = 0, M = 9.66e-5, De = 0$

**Viscoelastic Fluid** $Re = 80, \beta = 0.6, M = 9.66e-5, De = 10$

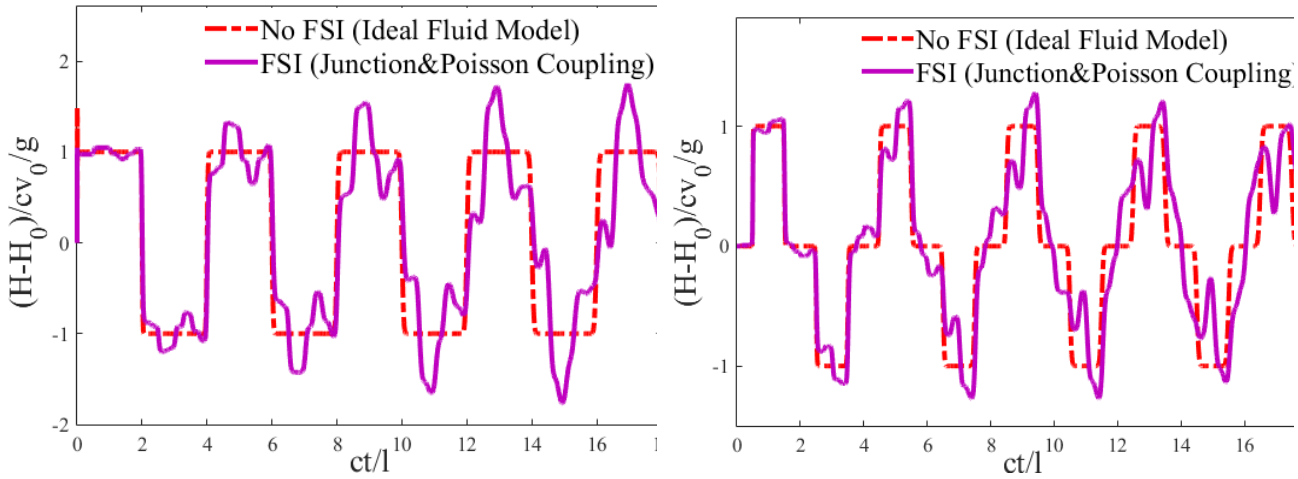


**A. At valve** **B. At midpoint**

**Fig. 14. Pressure time history during fluid hammer with ideal fluid in FSI junction& Poisson coupling**

Figs. 14 to 16 show the Poisson and junction coupling combined effects. In this state, due to the combination of two couplings, the behavioral complexity of the pressure wave is slightly higher but with precision in details, the precursor wave which travels ahead of the main wave of the fluid hammer can be recognized similarly to the junction coupling state and Poisson coupling state.

### 6- 4- Comparison of shear stresses due to fluid hammer phenomenon

In Fig. 17 a comparison between shear stresses due to fluid hammer phenomenon at the midpoint of the pipe with considering FSI Poisson and junction coupling is shown.

Fig. 17 in No FSI state shows that the shear stresses caused by fluid hammer with viscoelastic fluid is significantly reduced compared to the Newtonian state. Considering that the viscosity of the solutions are the same in both states, the reduction of shear stresses is related to viscoelastic fluid properties certainly. Storing of the potential energy in the viscoelastic solution due to the elastic properties of the solid character in it, can be considered the main factor in reducing the shear stresses in a viscoelastic solution compared to the Newtonian solution. It is clear that in an ideal fluid, the value of shear stress is zero. It seems that the effect of this property of viscoelastic fluid makes it possible to significantly reduce the severity of the initial shear stresses. Moreover, we know

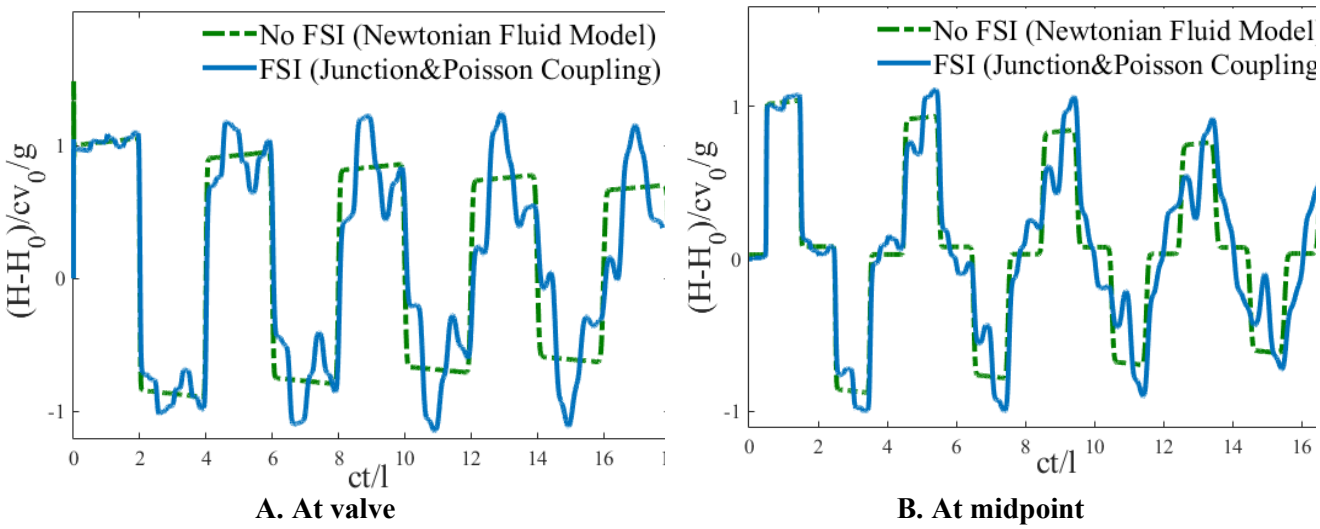


**Fig. 15. Pressure time history during fluid hammer with Newtonian fluid in FSI junction& Poisson coupling**

$\mathrm{Re}=80, \beta=0, De=0, M=9.66e-5$

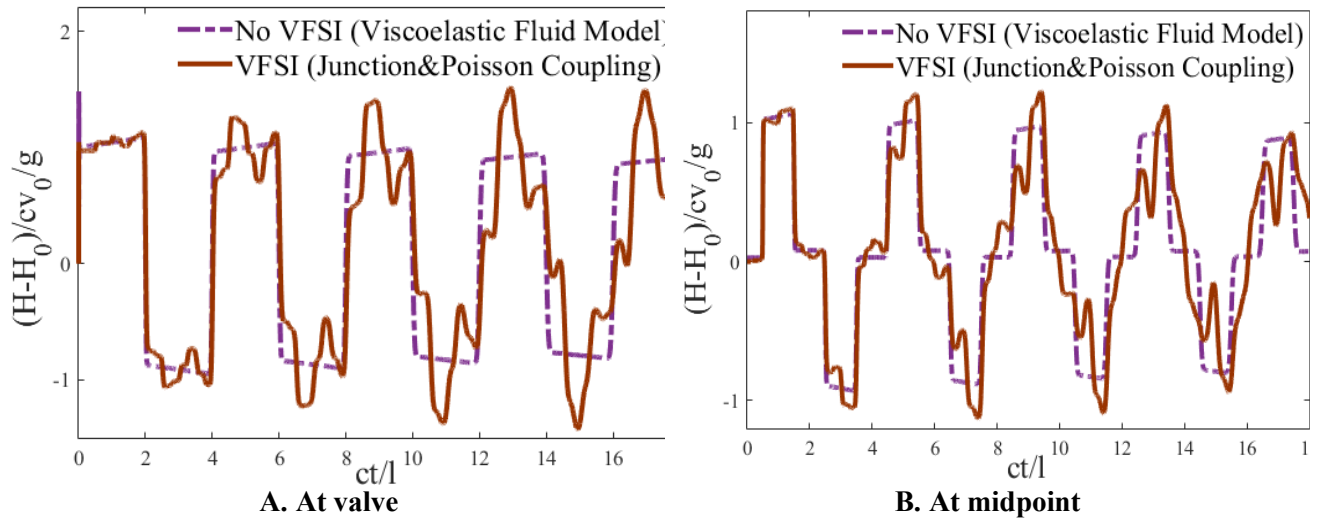


**Fig. 16. Pressure time history during fluid hammer with viscoelastic fluid in FSI junction& Poisson coupling**

$\mathrm{Re}=80, \beta=0.6, De=10, M=9.66e-5$

that the coupling effect increases the amount of shear stress to almost double. In Fig. 18 a comparison between shear stresses due to viscoelastic fluid hammer at the midpoint of the pipe is shown.

It's obvious that the VFSI, in contrast to the No VFSI model, causes intense pressures, high-frequency oscillations, and phase changes. Moreover, Fig. 18 shows that the value of imposed shear stresses due to Poisson coupling can be stated as the lowest shear stress among the other couplings. As can be seen that the junction coupling and the Poisson and junction coupling cause the highest shear stress along the pipe respectively.

## 7- Conclusions

The relationship between fluid-structure equations and constitutive equations for viscoelastic fluids during the fluid hammer phenomenon was investigated. Equations governing the problem include continuity and axial momentum for the fluid, and axial velocity and axial stress for the pipe. To model the viscoelastic fluid behavior, Oldroyd-B model relations were used. The LxF numerical method was also used to discretize the aforementioned equations. The system examined was a valve, pipe, and reservoir. The equations of junction and Poisson couplings and simultaneous coupling were defined with boundary conditions for each one. With a polymer

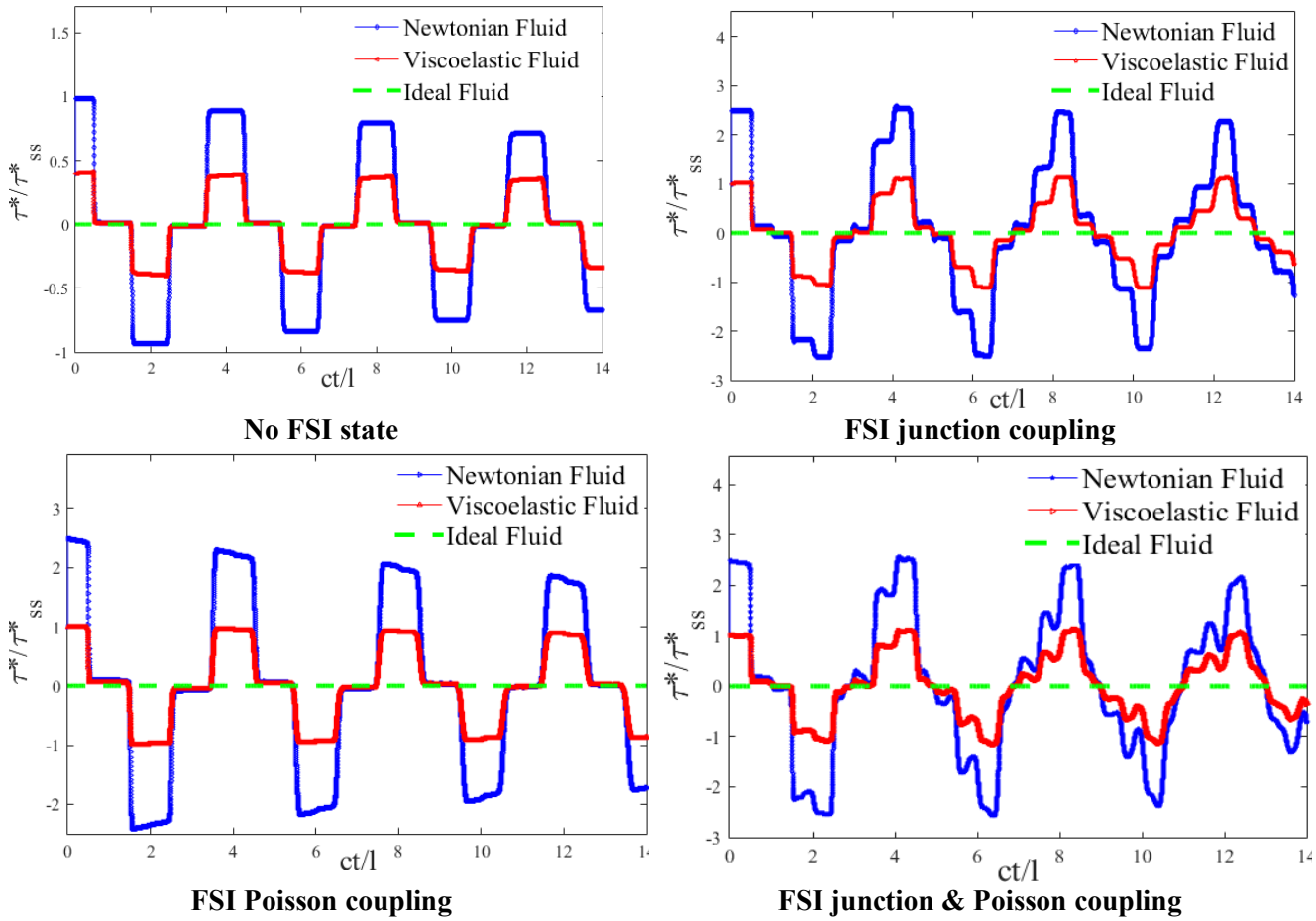


**Fig. 17. The comparison of shear stresses at the pipe midpoint**

**Newtonian Fluid** $\mathrm{Re}=80, \beta=0, M=9.66e-5, De=0$

**Viscoelastic Fluid** $\mathrm{Re}=80, \beta=0.6, M=9.66e-5, De=10$

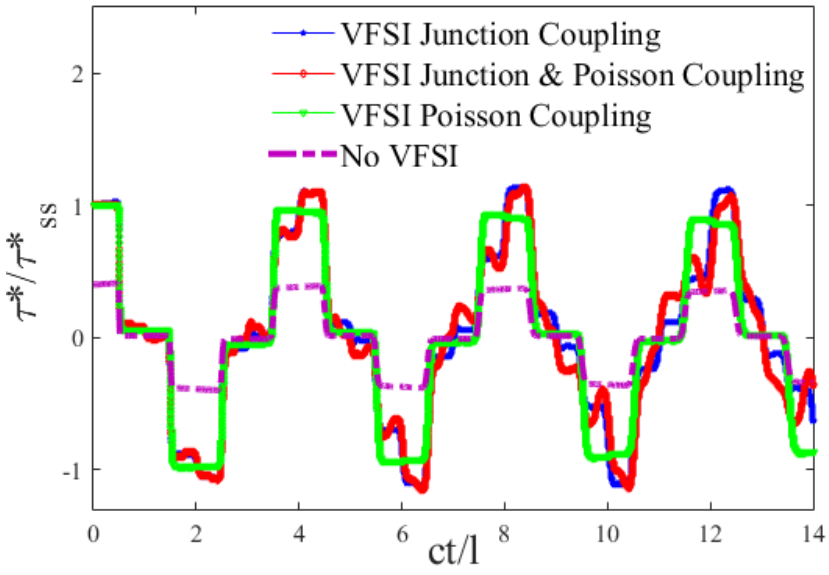


**Fig. 18. The comparison of shear stresses during viscoelastic fluid hammer at the midpoint**

of specific physical properties flowing in the pipe, the behavior of the polymer pressure head due to a sudden clogging of the valve was investigated in the case of couplings at the valve and midpoint of the pipe. Considering the effects of each coupling, shear stresses due to the fluid hammer phenomenon were calculated for the aforementioned viscoelastic fluid and the results were compared to a Newtonian fluid with similar viscosity. The results showed that viscoelastic fluid properties result in a significant reduction of the shear stress caused by this phenomenon. Moreover, the investigation of the pressure wave in couplings showed that junction coupling and compound coupling have a greater effect in increasing the pressure wave head and impose more shear stresses than the Poisson coupling along the pipe.

Appendix

Non-dimensionalization fluid and structure equations:

$$\bar{V}^* = \frac{\bar{V}}{v_0}, H^* = \frac{H}{c_f v_0 / g}, \quad z^* = \frac{z}{D}, t^* = \frac{t}{D/c_f}, \bar{\tau}^* = \frac{\bar{\tau}}{\rho c_f v_0} \tag{1-A}$$

$$De = \frac{\lambda}{D/v_0}, \quad \beta = \frac{\eta_p}{\eta_p + \eta_s}, \quad M = \frac{v_0}{c_f}, \quad \mathrm{Re} = \frac{\rho v_0 D}{\eta_p + \eta_s} \tag{2-A}$$

$$\dot{u}_z^* = \frac{\dot{u}_z}{v_0}, \sigma_z^* = \frac{\sigma_z}{\rho_t c_t v_0}, \quad c^* = \frac{c_f}{c_t}, \rho^* = \frac{\rho_f}{\rho_t}, D^* = \frac{D}{e} \tag{3-A-}$$

## Nomenclature

| | |
|---|---|
| $c$ | wave speed (m/s) |
| $D$ | pipe diameter (m) |
| $De$ | Deborah number |
| $E$ | Bulk modulus of compressibility (Pa) |
| $f$ | Darcy-Weisbach friction factor |
| $e$ | Pipe thickness (m) |
| $g$ | gravity acceleration (m/s$^2$) |

**Greek symbols**

| | |
|---|---|
| $\eta$ | viscosity (Pa.s) |
| $\boldsymbol{\tau}$ | Stress Tensor (Pa) |
| $\overset{\nabla}{\boldsymbol{\tau}}$ | Upper convected derivative of the stress tensor (Pa) |
| $\rho$ | Density (kg/m$^3$) |
| $\bar{\tau}_{rz}$ | Average stress components in the liquid in the corresponding surface and directions (Pa) |
| $\bar{\tau}_{zz}$ | Average stress components in the liquid in the corresponding surface and directions (Pa) |
| $\delta$ | The thickness of the boundary layer (m) |
| $\bar{\tau}$ | Average stress (Pa) |
| $\lambda$ | Relaxation time (s) |
| $\upsilon$ | Poisson's ratio |
| $H$ | pressure head (m) |
| $k$ | The coefficient of restriction for axial pipe movement |
| $M$ | Mach number |
| $p$ | Pressure (Pa) |
| $R$ | Pipe Radius (m) |
| | Reynolds number |
| $v_0$ | Velocity in steady-state (m/s) |
| $\bar{V}$ | Average cross-sectional velocity (m/s) |

**Superscripts**

| | |
|---|---|
| $n$ | Previous time steps |
| $n$ | |
| $+$ | next time steps |
| $1$ | |

**Subscripts**

| | |
|---|---|
| $f$ | fluid |
| $p$ | pipe material |
| $r$ | Radial direction |
| $z$ | Axial direction |

## References


[1] D. Korteweg, Ueber die Fortpflanzungsgeschwindigkeit des Schalles in elastischen Röhren, Annalen der Physik, 241(1878), 525–542.

[2] H. Helmholtz, Report on theoretical acoustics concerning works of the years 1848 and 1849, Gesammelte wissenschaftliche Abhandlungen 1(1882), 233–255.

[3] R. Skalak R, An extension of the theory of water hammer. Tech. rep. Columbia Univ. New York Dept of Civil Engineering and Engineering Mechanics, (1954).

[4] D.Wilkinson, The Dynamic Response of Pipework Systems to Water Hammer, (1980).

[5] J. Walker, J. Phillips, Pulse propagation in fluid-filled tubes. Journal of Applied Mechanics 44(1977), 31–35.

[6] R A.Valentin R A, J. Phillips, J. S Walker, Reflection and transmission of fluid transients at an elbow. Tech. rep., Argonne National Lab., IL (USA), (1979).

[7] D. Wiggert, F. Hatfield, S. Stuckenbruck, Analysis of liquid and structural transients in piping by the method of characteristics, (1987).

[8] D. Wiggert, Coupled transient flow and structural motion in liquid-filled pipingsystems: a survey. In: Proceedings of the ASME Pressure Vessels and Piping Conference. Chicago, USA, (1986).

[9] I-B. Joung, Y. Shin , A new model on transient wave propagation in fluid-filled tubes, Journal of Pressure Vessel Technology, 109(1987) 88–93.

[10] W. Bürmann, H. Thielen, Measurement and computation of dynamic reactive forces on pipes containing flow. Three R Int;(Germany, Federal Republic of), 27(1988).

[11] D. Wiggert, A. Tijsseling, Fluid transients and fluid-structure interaction in flexible liquid-filled piping, Applied Mechanics Reviews 54(2001) 455–481.

[12] A. Tijsseling, Exact solution of linear hyperbolic four-equation system in axial liquid-pipe vibration, Journal of Fluids and Structures 18 (2003), 179–196.

[13] A. Keramat, A. Tijsseling, Waterhammer with column separation, fluid-structure interaction and unsteady friction in a viscoelastic pipe, International Conference on Pressure Surges, Lisbon, Portugal, (2012).

[14] A. Keramat, A. Tijsseling, Q. Hou, A. Ahmadi, Fluid-structure interaction with pipe-wall viscoelasticity during water hammer, Journal of Fluids and Structures, 28 (2012), 434–455.

[15] L. Hadj-Taïeb, E. Hadj-Taïeb, Numerical simulation of transient flows in viscoelastic pipes with vapor cavitation. International Journal of Modelling and Simulation 29(2009), 206–213.

[16] F. Khalighi, A. Ahmadi, A. Keramat, Investigation of Fluid-structure Interaction by Explicit Central Finite Difference Methods, Int. J. Eng. Trans. B Appl, 29 (2016) 590-598.

[17] A. Groisman, M. Enzelberger, S. Quake, Microfluidic Memory and Control Devices, Sci., 300(2003), 955-958.

[18] [18] A. Morozov, W. Saarloos, Non-equilibrium physics: From complex fluids to biological systems I. Instabilities and pattern formation, Phys. Reports, 447(2007), 112 – 143.

[19] S. Sedussuriya, A. Jwilliams , C. Bailey, A cell-centred finite volume method for modelling viscoelastic flow, J. Non-Newtonian Fluid Mech., 117(2004), 42-61.

[20] E. Wahba, Runge–Kutta time-stepping schemes with TVD central differencing for the water hammer equations, International journal for numerical methods in fluids, 52(5) (2006) 571-590.

[21] D. F. Segura Fluid-structure interaction during hydraulic transients in pressurized pipes: experimental and numerical analyses, Laboratoire de Constructions Hydrauliques, (2016).

[22] E. Wahba, Non-Newtonian fluid hammer in elastic circular pipes: Shear-thinning and shear-thickening effects, Journal of Non-Newtonian Fluid Mechanics, 198 (2013) 24-30.

[23] D. Niedziela. On numerical simulations of viscoelastic fluids", Phd thesis, Naturwissenschaften, (2006).

[24] R.B. Bird, R.C. Armstrong, O. Hassager, Dynamics of polymeric liquids. Vol. 1: Fluid mechanics, (1987).

[25] L.F. Shampine, Two-step Lax–Friedrichs method, Applied Mathematics Letters, 18(10) (2005) 1134-1136.

[26] E. Holmboe, W. Rouleau, The effect of viscous shear on transients in liquid lines, Journal of Basic Engineering, 89(1) (1967) 174-180.

[27] E. Wahba, Modelling the attenuation of laminar fluid transients in piping systems, Applied Mathematical Modelling, 32(12) (2008) 2863-2871.

[28] E. Wahba, Modelling the attenuation of laminar fluid transients in piping systems, Applied Mathematical Modelling, 32(12) (2008) 2863-2871.

[29] B. Norouzi B., A. Ahmadi, M. Norouzi & M. Lashkarbolouk, Numerical modeling of the fluid hammer phenomenon of viscoelastic flow in pipes, Journal of the Brazilian Society of Mechanical Sciences and Engineering. 41(2019), 543-557.

[30] B. Norouzi, A. Ahmadi, M. Norouzi, M. LashkarBolook, Modeling of an Upper-Convected-Maxwell fluid hammer phenomenon in the pipe system, AUT Journal of Mechanical Engineering. 4(2020); 31-40.

[31] A. Bergant, A.S.Tijsseling, J.P. Vítkovský, D. Covas, A.R. Simpson, and M.F. Lambert, , Parameters affecting water hammer wave attenuation, shape and timing. Part 2: Case studies, Journal of Hydraulic Research, IAHR, 46(2008), 382–391.

**HOW TO CITE THIS ARTICLE**

*B. Norouzi, A. Ahmadi, M. Norouzi, M. Lashkarbolouk , Fluid-Structure Interaction During Viscoelastic Fluid Hammer Phenomenon in the Pipes, AUT J. Mech Eng., 6 (1) (2022) 95-112.*

**DOI:** 10.22060/ajme.2021.20217.5994